Journal of Inorganic Biochemistry 191 (2019) 21–28

Contents lists available at ScienceDirect

Journal of Inorganic Biochemistry

journal homepage: www.elsevier.com/locate/jinorgbio

Novel Co(II) and Cu(II) coordination complexes constructed from pyrazole-acetamide: Effect of hydrogen bonding on the self assembly process and antioxidant activity

Karim Chkirate[a], Saad Fettach[b], Khalid Karrouchi[c], Nada Kheira Sebbar[a], El Mokhtar Essassi[a], Joel T. Mague[d], Smaail Radi[e], My El Abbes Faouzi[b], N.N. Adarsh[f], Yann Garcia[f,*]

[a] LCOH, Département de Chimie, Faculté des Sciences, Université Mohamed V, BP1014, Rabat 10100, Morocco
[b] Laboratory of Pharmacology and Toxicology, Pharmacokinetic Research Team, Faculty of Medicine and Pharmacy, University Mohammed V, Rabat, Morocco
[c] LNCM, Direction du Médicament et de la Pharmacie, Ministère de la Santé, BP 6206, Rabat 10100, Morocco
[d] Department of Chemistry, Tulane University, New Orleans, LA 70118, USA
[e] LCAE, Département de Chimie, Faculté des Sciences, Université Mohamed I, BP 524, 60 000 Oujda, Morocco
[f] Institute of Condensed Matter and Nanosciences, Université catholique de Louvain, Place L. Pasteur 1, 1348 Louvain-la-Neuve, Belgium

ARTICLE INFO

Keywords:
Pyrazole
Crystal engineering
Coordination complexes
Hydrogen bonding
Antioxidant activity

ABSTRACT

In the present study, two pyrazole-acetamide derivatives namely *N*-(2-aminophenyl)-2-(5-methyl-*1H*-pyrazol-3-yl) acetamide (**L1**) and (*E*)-*N*-(2-(1-(2-hydroxy-6-methyl-4-oxo-*4H*-pyran-3-yl)ethylideneamino)phenyl)-2-(5-methyl-*1H*-pyrazol-3-yl) acetamide (**L2**) have been synthesized and characterized by infrared spectrophotometry (IR), nuclear magnetic resonance spectroscopy (NMR) and electrospray ionization-mass spectrometry (ESI-MS). Two coordination complexes of **L1** and **L2**, namely $[Co(\mathbf{L1})_2(EtOH)_2]\cdot Cl_2$ (**1**) and $[Cu(\mathbf{L2})]\cdot H_2O$ (**2**), respectively have been synthesized and characterized by elemental analysis and spectroscopic studies. The solid state structure of these two complexes was established by single crystal X-ray crystallography. In complex **1**, the amide O and pyrazole N atoms of two molecules of **L1** take part in coordination with octahedral Co(II) ions, the remaining two coordination sites being occupied by two EtOH molecules leading to a N_2O_4 coordination environment. On the other hand, the imine N atoms, pyrazole N and O atoms of the 2-hydroxy-6-methyl-4H-pyran-4-one function present in **L2** are involved in coordination with Cu(II) ions, resulting in a distorted square planar geometry displaying a N_2O_4 chromophore, in complex **2**. The crystal packing analysis of **1** and **2**, revealed 1D and 2D supramolecular architectures respectively, *via* various hydrogen bonding interactions, which are discussed in the present account. Furthermore, the antioxidant activity of the ligands and their complexes were determined *in vitro* by 1,1-diphenyl-2-picrylhydrazyl (DPPH), 2,2′-azino-bis(3-ethylbenzothiazoline-6-sulphonic acid (ABTS) and ferric reducing antioxidant power (FRAP), showing that the ligands **L1** and **L2** and complexes **1** and **2** present significant antioxidant activity.

1. Introduction

Pyrazole derivatives are biologically active heterocyclic compounds [1]. This substance class has been the topic of numerous pharmaceutical studies being used for their medicinal properties such as anti-inflammatory [2,3], antimicrobial [4], antiviral [5], analgesic [6], antitumoral [7], catecholase [8], and even as insecticides [9]. Some of the specific examples, including pyrazoles, inhibit the secretion of amyloid responsible for Alzheimer's disease [10]. Other examples are pyrazolopyrimidines [11] reported as estrogen receptor antagonists. In particular, pyrazolylacetamide derivatives have been evaluated for their *in vitro* activity as antimycobacterial agents against Mycobacterium smegmatis and as anti-cytotoxic anti-tuberculosis agents [12] and also as anti-glycemic agents [13]. They also have therapeutic properties for the treatment of Cryptosporidium parasites [14]. Their metal complexes have proven antimicrobial activities [15] too and may also have applications in catalysis [16].

Nitrogen systems have attracted more attention in recent years because of their interesting properties in coordination chemistry [17,18], particularly the synthesis of iron complexes due to their spin crossover [19] and their molecular properties [20]. This ability is mainly due to the presence of hybrid sp^2 nitrogen donors [21] with the involvement,

* Corresponding author.
E-mail address: yann.garcia@uclouvain.be (Y. Garcia).

https://doi.org/10.1016/j.jinorgbio.2018.11.006
Received 12 September 2018; Received in revised form 29 October 2018; Accepted 8 November 2018
Available online 09 November 2018
0162-0134/

in some cases, of other donating sites such as oxygen and sulfur atoms [22].

Reactive oxygen species (ROS) are chemically reactive chemical species containing oxygen. However, the excess production of ROS can become toxic to the major components of the cell, lipids, proteins and nucleic acids, and can give rise to oxidative stress that can be involved in various pathologies [23,24].

Antioxidant pharmacotherapy has appeared as a tool to minimize the bimolecular damage caused by the attack of ROS to these vital constituents of living organisms, and therefore synthetic antioxidants have received much attention from the pharmaceutical viewpoint [3]. However, a significant number of research teams have concentrated on the role of complexes as antioxidants [25,26].

In order to search for new ligand candidates for assemblies of metal complexes, we considered the case of pyrazole acetamide ligands with O and N donor atoms. These molecules are particularly interesting as ligands for the construction of polynuclear complexes as models for bioinorganic systems [27,28]. In this work, we describe the synthesis of derivatives of pyrazole functionalized with acetamides and the crystal structure of two novel Co(II) and Cu(II) coordination complexes derived from these ligands, namely *N*-(2-aminophenyl)-2-(5-methyl-*1H*-pyrazol-3-yl) acetamide (**L1**) and (*E*)-*N*-(2-(1-(2-hydroxy-6-methyl-4-oxo-*4H*-pyran-3-yl)ethylideneamino)phenyl)-2-(5-methyl-*1H*-pyrazol-3-yl) acetamide (**L2**) (Fig. 1). The antioxidant properties of the ligands and their complexes are evaluated *in vitro* using DPPH(1,1-diphenyl-2-picrylhydrazyl) and ABTS(2,2'-azino-bis(3-ethylbenzothiazoline-6-sulphonic acid) radical scavenging methods and Ferric Reducing Antioxidant Power (FRAP).

2. Experimental

2.1. General methods

Melting points were measured using a Büchi B-545 digital capillary melting point apparatus and used without correction. Reactions were checked with TLC using aluminum sheets with silica gel 60 F254 from Merck. IR spectra were recorded on a Perkin-Elmer VERTEX 70 FT-IR spectrometer covering field 400–4000 cm^{-1}. ^1H and ^{13}C NMR spectra were recorded in DMSO-d_6 on a Bruker spectrometer (300 MHz). Chemical shifts are expressed in ppm by using tetramethylsilane (TMS) as internal reference. Mass spectra were collected using an API 3200 LC/MS/MS system, equipped with an ESI source. Chemical reagents were purchased from Fluka, Sigma and Aldrich chemicals.

2.2. Synthesis

2.2.1. Synthesis of (Z)-4-(2-oxopropylidene)-4,5-dihydro-1H-benzo[b][1,4]diazepin-2(3H)-one

0.02 mol (3.36 g) of dehydroacetic acid and 0.04 mol (4.32 g) of *o*-phenylenediamine were refluxed in xylene (80 mL) for 4 h. Next, the precipitated product was filtered under reduced pressure and then recrystallized in ethanol. Yield: 75%; M.p (°C): 236–238; IR (ATR, v (cm^{-1})): 1671, 1607, 1575; ^1H NMR (300 MHz, DMSO-d_6, δ(ppm)): 2.00 (s, 3H, CH_3); 3.00 (s, 2H, $-CH_2$); 5.20 (1H, s); 7.10 (4H, m); MS: m/z = 216 $(M + H)^+$.

2.2.2. Synthesis of N-(2-aminophenyl)-2-(5-methyl-1H-pyrazol-3-yl) acetamide (L1)

2 g of (Z)-4-(2-oxopropylidene)-4,5-dihydro-*1H*-benzo[*b*][1,4] diazepin-2(*3H*)-one and stoichiometric amount of hydrazine were refluxed in ethanol (40 mL) for 2 h. After concentration of the solvent volume to 20 mL, the solution was allowed to stand; the precipitate formed was filtered off and then recrystallized in ethanol. A single crystal was obtained after recrystallization from ethanol. Yield: 80%; M.p (°C): 170–172; IR (ATR, v(cm^{-1})): 3000–3400 (NH, NH_2), 1737 (C═O); 1655 (C═N); ^1H NMR (300 MHz, DMSO-d_6, δ(ppm)): 2.51 (s, 3H, CH_3), 2.20 (s, 2H, CH_2), 4.86 (s, 2H, NH_2), 5.94 (s, 1H, H-pyrazole), 6.52–7.16 (m, 5H, H−Ar), 9.25 (s, 1H N−H (amide), 12.24 (s, 1H, NH-pyrazole); MS: m/z = 230 $(M + H)^+$.

2.2.3. Synthesis of (E)-N-(2-(1-(2-hydroxy-6-methyl-4-oxo-4H-pyran-3-yl) ethylideneamino)phenyl)-2-(5-methyl-1H-pyrazol)-3-yl) acetamide (L2)

To a solution of 5 mmol of *N*-2-aminophenyl-5-methyl-pyrazol-3-yl acetamide in ethanol (60 mL), 5 mmol of dehydroacetic acid solubilized in ethanol was slowly added. After 24 h stirring at room temperature, the formed precipitate was filtered, washed with ethanol and dried under vacuum. Yield: 85%; M.p. (°C) = 204–206; IR (ATR, v(cm^{-1})): 3390 (OH), 3203–3145 (NH), 1700–1710 (C═O), 1590–1610 (C═N); ^1H NMR (300 MHz, DMSO-d_6, δ(ppm)): 2.14 (s, 3H, CH_3); 2.37 (s, 3H, CH_3); 2.51 (s, 3H, CH_3); 3.33 (s, 2H, CH_2); 5.81 (s, 1H, H4-pyrazole); 5.84 (s, 1H, pyrone); 7.39–7.55 (m, 4H, phenyl); 9.21 (s, 1H, NH-CO); 12.17 (s, 1H, NH-pyrazole); 15.49 (s, 1H, OH); MS: m/z = 380.4 $(M + H)^+$.

2.2.4. Synthesis of $[Co(L1)_2(EtOH)_2]\cdot Cl_2$ (1)

L1 (14.4 mg, 0.07 mmol, 2 equiv) was dissolved in ethanol (5 mL). $CoCl_2\cdot 6H_2O$ (7.5 mg, 0.04 mmol, 1 equiv) was dissolved in ethanol (5 mL) and added to the above solution of **L1**. The resulting light brown solution was left at room temperature. Single crystals were obtained by slow evaporation of a clear light brown solution of the reaction mixture after 24 h. Yield: 48%.

2.2.5. Synthesis of $[Cu(L2)]\cdot H_2O$ (2)

L2 (80 mg, 0.25 mmol, 1 equiv) was dissolved in MeOH (5 mL). $CuSO_4\cdot 5H_2O$ (62.4 mg, 0.25 mmol, 1 equiv) was dissolved in water (5 mL) and added to the **L2** solution above. The resulting solution was stirred and warmed slightly. After a few moments, a dark green precipitate was deposited. The precipitate was filtered and then recrystallized from acetonitrile and left at room temperature. Dark green single crystals were obtained by slow evaporation of the reaction mixture after 24 h. Yield: 30%.

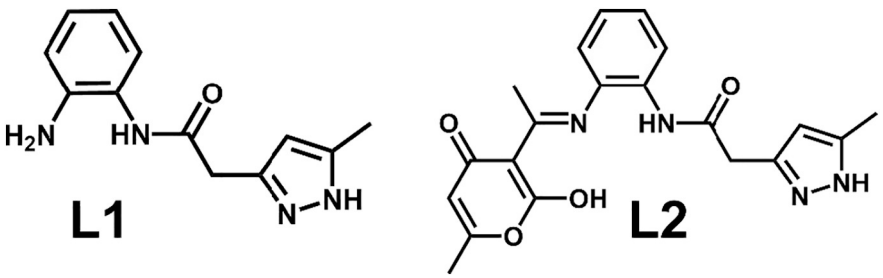

Fig. 1. *N*-(2-Aminophenyl)-2-(5-methyl-*1H*-pyrazol-3-yl) acetamide (**L1**) and (*E*)-*N*-(2-(1-(2-hydroxy-6-methyl-4-oxo-*4H*-pyran-3-yl)ethylideneamino) phenyl)-2-(5-methyl-*1H*-pyrazol-3-yl) acetamide (**L2**).

Table 1
Crystallographic and refinement data for **1** and **2**.

	1	2
CCDC number	**1853218**	**1853219**
Empirical formula	$C_{28}H_{40}CoN_8O_4Cl_2$	$C_{20}H_{20}CuN_4O_5$
Formula weight	682.51	459.9
Crystal size (mm)	0.41 × 0.18 × 0.14	0.44 × 0.24 × 0.23
Crystal system	Triclinic	Triclinic
Space group	*P*1̄	*P*1̄
a (Å)	8.3807(10)	10.0686(7)
b (Å)	9.5420(12)	11.5591(8)
c (Å)	11.0152(14)	17.1250(11)
α (°)	73.026(2)	85.925(1)
β (°)	71.246(2)	78.880(1)
γ (°)	78.313(2)	72.506(1)
V (Å^3)	792.00(17)	1865.0(2)
Z	1	4
$D_{calc.}$ (g/cm^3)	1.431	1.638
F(0 0 0)	357	948
μMoKα (cm^{-1})	0.758	1.215
T (K)	100(2)	100(2)
Range of h, k, l	−11/11, −13/13, −15/15	−13/13, −16/15, −23/23
θ min/max	2.01/29.59	1.85/29.63
Reflections collected/ unique/observed	15,439/4295/3739	36,628/10116/9042
Data/restraints/ parameters	4295/0/198	10,116/0/701
Goodness-of-Fit (GOF) on F^2	1.148	1.044
Final R indices [I > 2σ(I)]	R1 = 0.0349 wR2 = 0.0977	R1 = 0.0290 wR2 = 0.0754
R indices (all data)	R1 = 0.0396 wR2 = 0.0998	R1 = 0.0334 wR2 = 0.0775

2.3. X-ray analysis

X-ray single-crystal data were collected on single crystals using Mo Kα (λ = 0.7107 Å) radiation on a Bruker SMART APEX diffractometer equipped with CCD area detector. Unit cell refinement data reduction (SAINT) and structure solution as well as refinement (SHELXL) [29] were carried out using the software package of SMART APEX. The structures **1** and **2** were solved by direct method and refined in a routine manner. In both structures, non-hydrogen atoms were treated anisotropically. In compound **1**, hydrogen atoms were geometrically fixed. On the other hand in **2**, hydrogen atoms were located on a difference Fourier map and refined. Molecular graphics were generated by using the softwares MERCURY 3.9 [30] and POV-Ray. The details of the X-ray crystal data and the structure solution as well as the refinement are given in Table 1. CCDC 1853218 and 1853219 for **1** and **2**, respectively contain the supplementary crystallographic data for these compounds, and can be obtained free of charge from the Cambridge Crystallographic Data Centre *via* www.ccdc.cam.ac.uk/data_request/cif.

2.4. Antioxidant activity

2.4.1. DPPH radical scavenging activity

The radical-scavenging activity of each synthesized compounds was evaluated on the basis of its activity in scavenging the stable DPPH radical, according to the method described by Li et al. [31]. In this procedure, 2 mL of a 4% solution of DPPH radical in methanol (w/v) was mixed with 500 μL of sample solutions at different concentrations (31–2000 μM).

The scavenging capacity was determined spectrophotometrically after 30 min of incubation by monitoring the decrease of the absorbance at 517 nm. Lower absorbance of the reaction mixture indicates higher free radical scavenging activity. Ascorbic acid was used as standard. The percent DPPH scavenging effect was calculated using the following equation:

$$\%\text{of scavenging} = [(A_c - A_t)/A_c] \times 100$$

where A_c is the absorbance of the control sample (DPPH solution without test sample) and A_t is the absorbance of the test sample (DPPH solution + test compound). Tests were performed in triplicate, and the results were averaged.

2.4.2. ABTS radical scavenging activity

The ABTS free radical-scavenging activity of our synthesized compounds was estimated using the method described by Tuberoso et al. [32]. The ABTS radical cation was produced by reacting ABTS with potassium persulfate. The blue-green ABTS was produced through the reaction between 7 mM ABTS and 70 mM potassium persulfate in water. The mixture was stored at room temperature in the dark for 16 h prior use. The ABTS solution was then diluted with 80% methanol to obtain an absorbance of 0.700 ± 0.005 at 734 nm. One hundred microliters of sample solutions at 1 mM were added to 2 mL of ABTS solution and the absorbance was recorded at 734 nm after 1 min incubation at room temperature. This was compared to the blank where 200 μL of the methanol was added to 2 mL of ABTS solution. A standard curve was obtained by using Trolox reference solution at various concentrations. The scavenging activities of different concentrations of synthesized compounds *vs.* ABTS radical were also measured to calculate the IC50, and the procedure was similar to the DPPH scavenging method described above. The test was carried out in triplicate and IC50 values were reported as means ± SD.

$$\%\text{Inhibition} = (A_c - A_t/A_c)/100$$

where A_c is the absorbance of the control and A_t is the absorbance in the presence of the samples or reference. The control did not contain compound or standard.

2.4.3. Ferric reducing/antioxidant power (FRAP) assay

The ferric-reducing capacity of the ligands and complexes was investigated by using the potassium ferricyanide-ferric chloride method with some modifications [33]. Briefly, the sample (1 mL) at 1 mM/L was mixed with 2.5 mL of phosphate buffer (0.2 M, pH 6.6) and 2.5 mL of 1% potassium ferricyanide. The mixture was then incubated at 50 °C for 20 min to reduce ferricyanide into ferrocyanide. A portion (2.5 mL) of trichloroacetic acid (10%) was added to the mixture which was then centrifuged at 3000 rpm for 10 min. Finally, 2.5 mL of the supernatant was mixed with 2.5 mL of distilled water and 0.5 mL $FeCl_3$ solution (0.1%, w/v), and the absorbance was measured at 700 nm. Increased absorbance values indicate a higher reducing power. The results were expressed as ascorbic acid equivalent per mM of compound (μM/mM comp).

3. Result and discussion

3.1. Synthesis of pyrazole-acetamide ligands *L1* and *L2*

Our strategy was to develop a simple, high-yield, synthetic procedure in a few steps to prepare the desired acetamide derivatives. The development of the synthesis of **L1** and **L2** is given in Scheme 1.

The major product **3** [34] was produced in good yield by condensation of *o*-phenylenediamine with dehydroacetic acid (DHA) in refluxing xylene for 4 h. The second step was to react on product **3** hydrazine monohydrate as a reagent in stoichiometric amount in ethanol, reflux for 2 h to give the pyrazole-acetamide **L1** ligand in good yield [35]. The third step was to react on **L1** DHA in ethanol at room temperature for 24 h to afford the pyranylpyrazole acetamide ligand **L2**, again in good yield (Scheme 1).

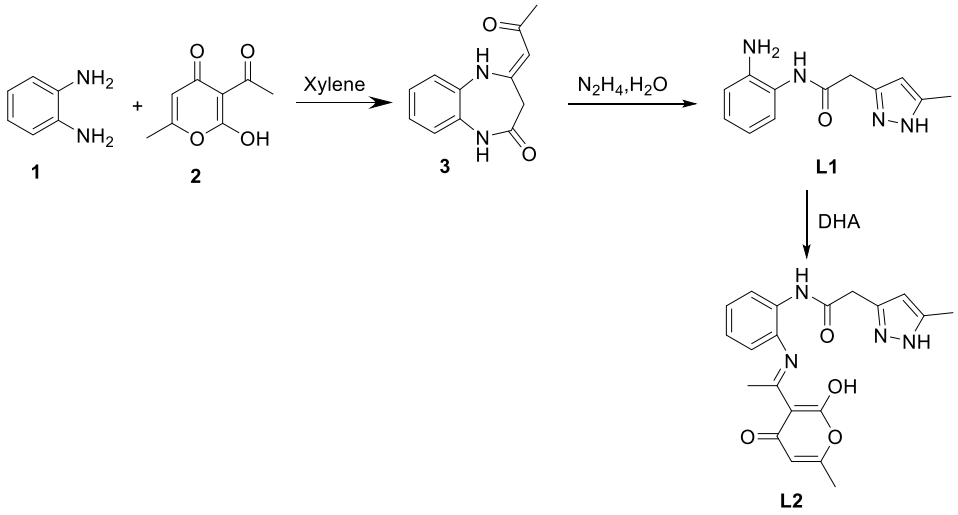

Scheme 1. Synthetic routes of **L1** and **L2**.

Table 2
Hydrogen bonding parameters of **1** and **2**.

D—H···A	D—H (Å)	H···A (Å)	D···A (Å)	D—H···A (°)	Symmetry operation for A
1					
N(2)—H(2)···N(4)	0.91	2.07	2.9801(18)	175	1 − x, 1 − y, 1 − z
O(2)—H(2A)···Cl(1)	0.87	2.20	3.0575(12)	168	x, y, z
N(3)—H(3A)···Cl(1)	0.91	2.24	3.1468(14)	175	1 − x, −y, 1 − z
N(4)—H(4A)···Cl(1)	0.91	2.46	3.2981(13)	153	x, y, z
N(4)—H(4B)···Cl(1)	0.91	2.48	3.3779(14)	171	2 − x, −y, 1 − z
2					
N(1)—H(1)···O(9)	0.80(2)	2.21(2)	2.905(2)	146(2)	1 − x, 1 − y, 1 − z
N(5)—H(5)···O(10)	0.81(3)	1.99(3)	2.759(2)	158(2)	1 + x, y, z
O(9)—H(9A)···O(1)	0.84(3)	1.92(3)	2.7508(19)	171(2)	−x, 1 − y, 1 − z
O(9)—H(9B)···O(6)	0.86(3)	2.16(3)	2.9594(18)	155(3)	1 − x, −y, 1 − z
O(10)—H(10A)···O(5)	0.84(3)	1.88(3)	2.711(2)	170(3)	x, y, z
O(10)—H(10B)···O(1)	0.79(3)	2.04(3)	2.830(2)	171(3)	x, y, z
C(25)—H(25B)···O(2)	0.98(2)	2.29(2)	3.1658(19)	147.8(17)	x, −1 + y, z
C(31)—H(31)···O(7)	0.92(2)	2.52(2)	3.432(2)	170.3(17)	2 − x, −y, −z
C(39)—H(39)···O(5)	0.90(2)	2.57(2)	3.432(2)	161.4(18)	1 + x, y, z

*3.2. Synthesis of coordination complexes **1** and **2***

The crystallization of coordination compounds obtained the reaction of pyrazole-acetamide ligand **L1** and Co^{II} on one hand in an ethanolic solution (metal/ligand ratio 1:2) and the reaction of pyranyl pyrazole acetamide ligand **L2** with Cu^{II} on the other hand in an aqueous methanolic solution (metal/ligand ratio 1:1), followed by recrystallization in acetonitrile, afforded single crystals of two coordination complexes $[Co(\mathbf{L1})_2(EtOH)_2]\cdot Cl_2$ (**1**) and $[Cu(\mathbf{L2})]\cdot H_2O$ (**2**).

*3.3. Description of the crystal structures of the complexes $[Co(\mathbf{L1})_2(EtOH)_2]\cdot Cl_2$ (**1**) and $[Cu(\mathbf{L2})]\cdot H_2O$ (**2**)*

*3.3.1. $[Co(\mathbf{L1})_2(EtOH)_2]\cdot Cl_2$ (**1**)*

Single crystal X-ray diffraction analysis has shown that complex **1** crystallizes in centrosymmetric triclinic *P*1 space group (Table 1). The crystal structure of **1** can be described as a chloride inclusion coordination complex of Co(II). The asymmetric unit comprises one half of Co(II) (sitting on an inversion center), one molecule of **L1** and EtOH (both being coordinated to Co(II) and are around an inversion center) and one chloride counter anion (also found around an inversion center). Therefore the remaining ligand **L1** and the EtOH molecule for the coordination with Co(II) were generated by the symmetry inversion center present on the Co(II) atom. The Co(II) metal center exhibits distorted octahedral geometry [∠N—Co—O = 87.78(4)–92.22(4)°; ∠O—Co—O = 88.89(4)–91.11(4)°] with a CoN_2O_4 chromophore; the equatorial positions are coordinated by two molecules of ligand **L1** through the imine N atoms of pyrazole and O atoms of amide functionalities. Such coordination affords a stable six membered ring involving the Co(II) metal center and the ligand, due to the chelation effect of **L1**. The axial positions of Co(II) are occupied by O atoms of EtOH molecules. In the crystal structure, the ligand moiety displays a non-planar conformation as expected, in which the pyrazole and aromatic rings are away from a torsion angle of ~65.63° from each other. In fact such ligand conformation affords stability to the coordination complex, supported by intra-molecular hydrogen bonding interactions involving the $-NH_2$ and pyrazole functionalities [N—H···N = 2.9801(18)Å; ∠N—H—N = 175°]. The coordination complex **1**, was self-assembled *via* hydrogen bonding comprising of the lattice included Cl^- anion, amide N—H═O, amine $-NH_2$ and hydroxyl —OH *via* O—H···Cl and N—H···Cl interactions [O—H···Cl = 3.0575(12) Å, ∠O—H—Cl = 168°; N—H···Cl = 3.1468(14)–3.3779(14)Å, ∠N—⊖H—Cl = 153–175°] (Table 2). Such self-assembly of **1**, through the occluded Cl^- resulted in a one dimensional hydrogen bonded chain, which can be seen along the crystallographic axis "a". Further these chains are packed in parallel fashion supported by a weak C—H···π(ring) interaction (Fig. 2), which resulted in a 2D sheet structure, with the encapsulation of Cl^- within the void space. Interestingly such 2D sheets are further assembled in top of each other in an offset

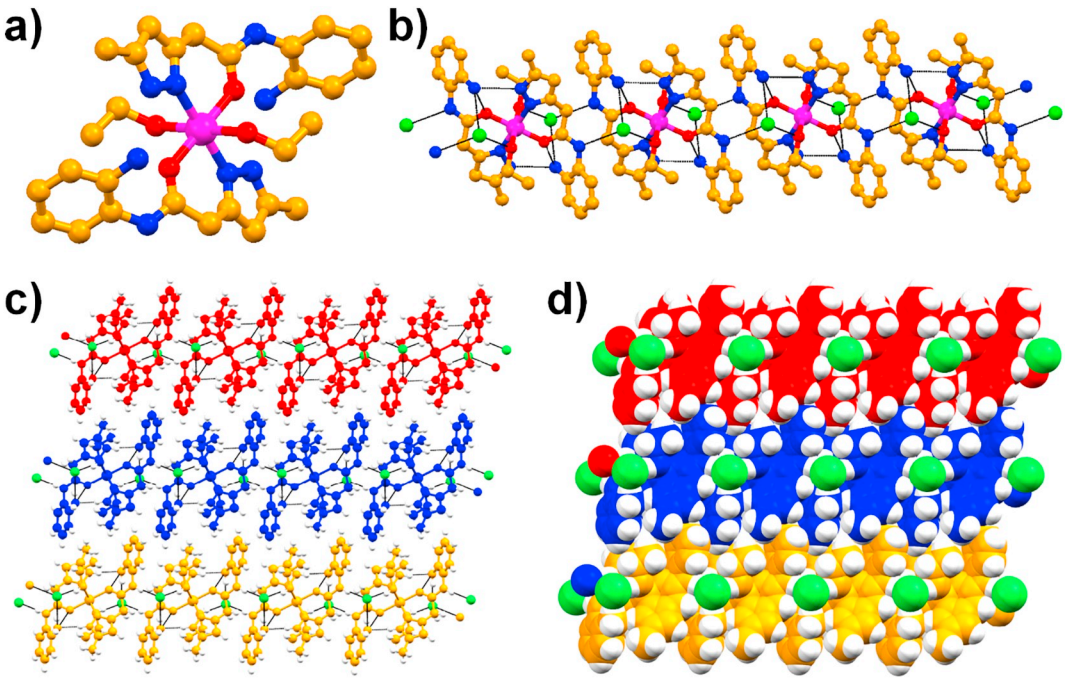

Fig. 2. Crystal structure description of **1**: a) crystal structure of the coordination complex showing the coordination environment; b) one dimensional (1D) hydrogen bonded chain supported by O—H···Cl and N—H···Cl interactions, displaying the inclusion of Cl^- anion; the parallel packing of 1D hydrogen bonded chains in ball and stick fashion c) and spacefill model d), (the adjacent chain are shown in red, blue and orange color, Cl^- is shown in green color).

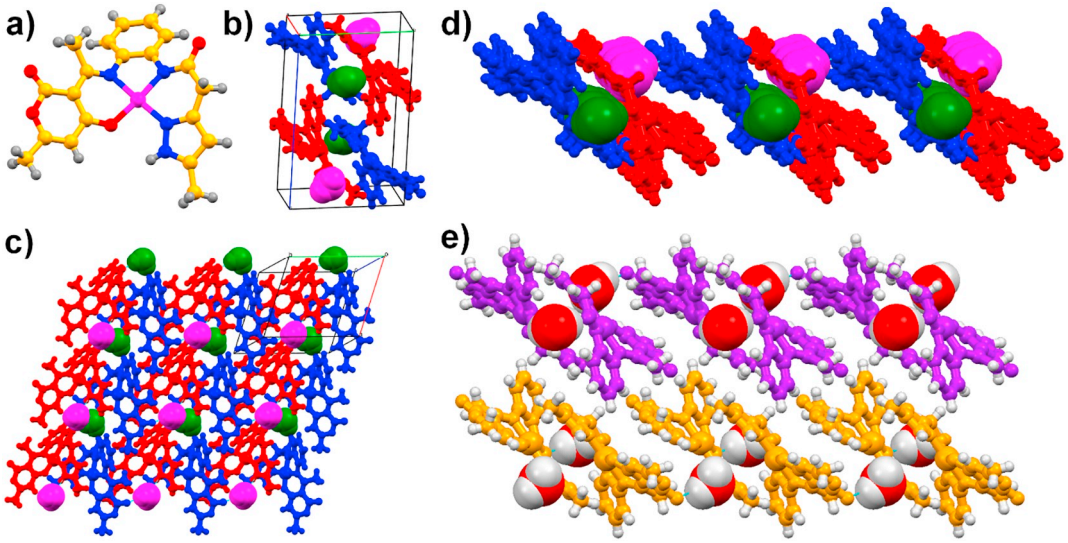

Fig. 3. Crystal structure description of **2**: a) crystal structure of the coordination complex showing the square planar coordination geometry; b) the packing of crystallographically independent molecules of complexes (shown in blue and red color) and occluded water (shown in magenta and green); 2D hydrogen bonded network, formed by the self-assembly of crystallographically independent molecules of complexes and water along crystallographic axis "c" (c) and "a" axis (d); e) offset packing of 2D sheets.

fashion, with the support of offset π···π stackings between pyrazolyl rings with centroid…centroid distances of 3.4976(19)Å (Fig. 2).

3.3.2. *[Cu(**L2**)]·H_2O (**2**)*

Dark red-violet colored column shaped single crystals of **2** crystallized in a centrosymmetric triclinic $P\bar{1}$ space group (Table 1). The asymmetric unit consists of two crystallographically independent molecules of coordination complex and a lattice included water molecule. Each complex molecules contains a Cu(II) metal center and one molecule of ligand coordinated to the metal center. The Cu(II) metal center shows distorted square planar geometry [∠N—Cu—O = 89.18(5)–91.81(5)°; ∠N—Co—N = 84.68(5)–94.14(5)°] having a four coordination with CuN_2O_2 coordination environment. In the crystal structure, the ligand **L2** showed reasonable non-planarity which is easily confirmed from the torsion angle between the aromatic ring and pyrazole ring, and the aromatic ring and 2-hydroxy-6-methyl-4H-pyran-4-one ring, such as ~43.66–44.97° and ~41.12–41.91°, respectively. Thus, the mononuclear Cu(II) complex **2**, exhibits non planar conformation. In the crystal structure of complex **2**, crystallographically independent molecules of complexes and water molecules are recognized each other through intermolecular hydrogen bonding *via* O—H···O and N—H···O [O–H···O = 2.711(2)–2.9594(18)Å, ∠O—H—O = 155(3)–171(2)°; N—H···O = 2.759(2)–2.905(2)Å, ∠N—H—O = 146(2)–158(2)°] interactions, which leads to the formation of a two dimensional (2D) corrugated

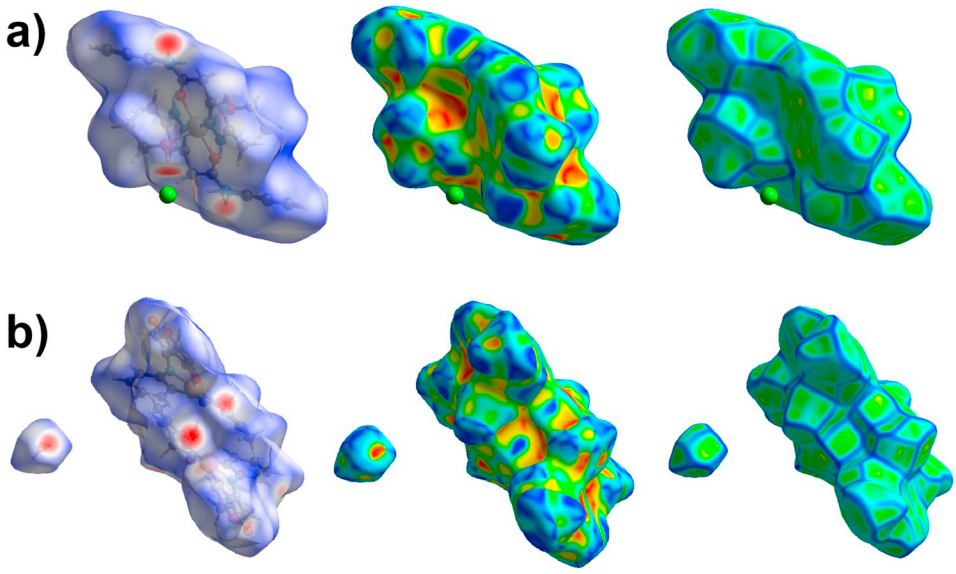

Fig. 4. Hirshfeld surface mapped having d_{norm} (left), shape index (middle), and curvedness (right) of **1** (a) and **2** (b).

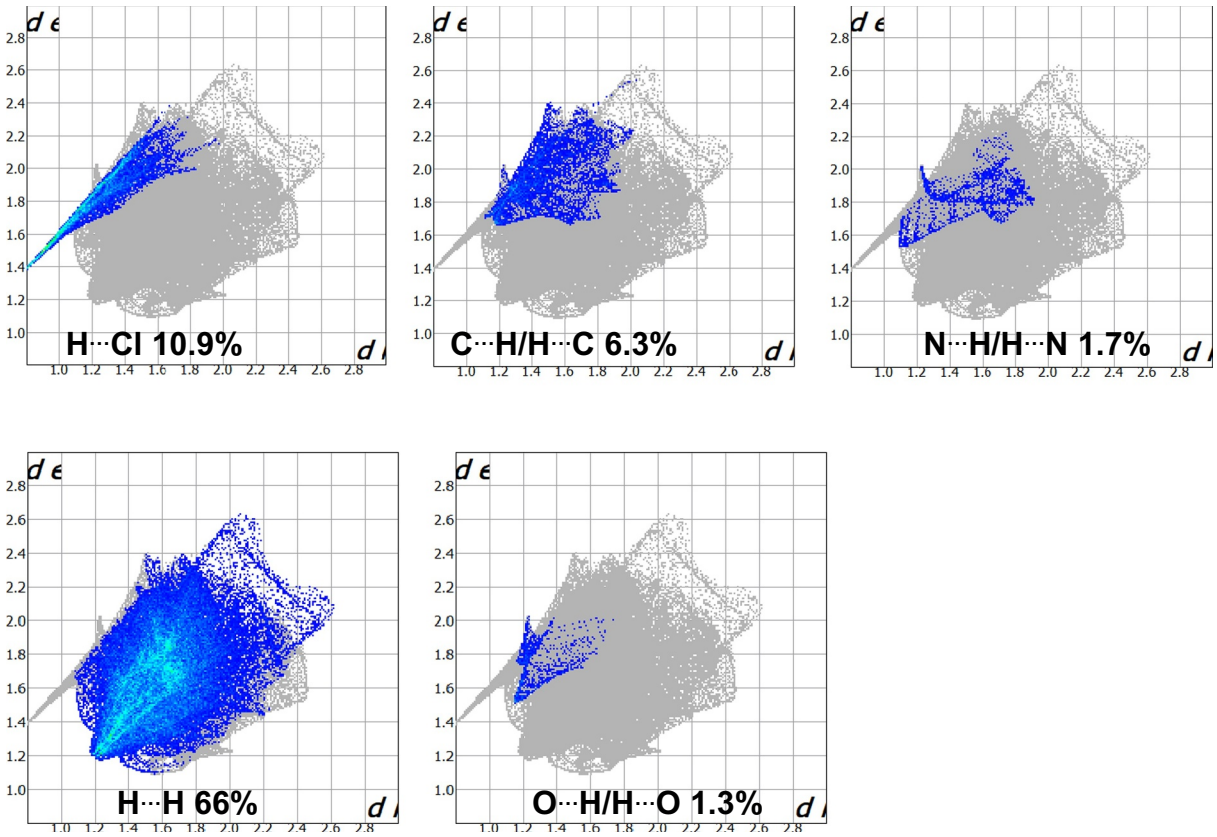

Fig. 5. The 2D fingerprint plots for **1**.

hydrogen bonded sheet (Table 2). Such 2D hydrogen bonded sheets are further packed on top of each other in an offset fashion, supported by weak intermolecular interactions (Fig. 3).

3.4. Hirshfeld surface analysis

Hirshfeld surface analysis was performed to calculate the intermolecular interactions present in the coordination complexes **1** and **2**, and the fingerprint plots were generated using CrystalExplorer 3.1 [36]. The following equation is used to calculate the normalized contact distance (d_{norm}), from the values of d_e (distance between the Hirshfeld surface and external molecule), d_i (distance between the Hirshfeld surface and inside molecule) and Van der waals radii of the atoms (r_i^{vdw} or r_e^{vdw}). The resultant value of d_{norm}, we can identify the regions participating in the intermolecular interactions in the complexes **1** and **2** [37].

$$d_{norm} = \frac{d_i - r_i^{vdw}}{r_i^{vdw}} + \frac{d_e - r_e^{vdw}}{r_e^{vdw}}$$

Moreover by using CrystalExplorer 3.1, we can plot a two

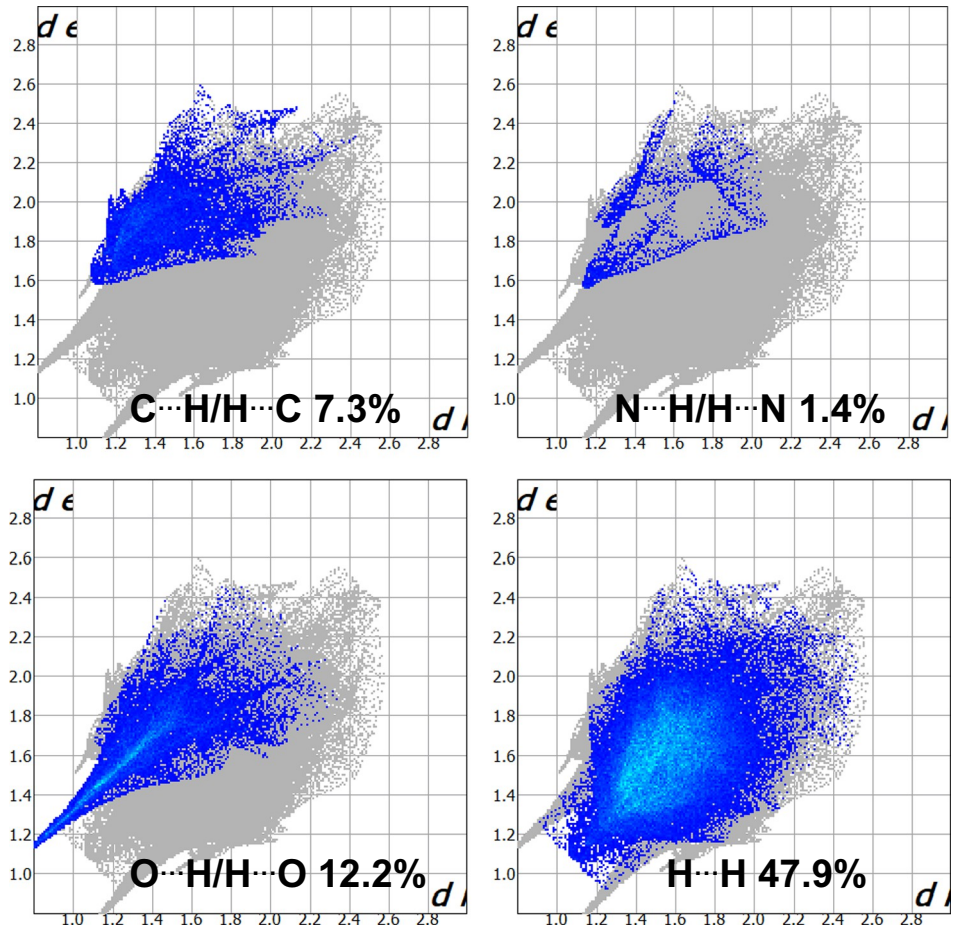

Fig. 6. The 2D fingerprint plots for **2**.

Table 3
Antioxidant activity of **L1**, **L2**, **1** and **2**.

	DPPH IC_{50} (μM)	ABTS μM ET/mM	FRAP μM EAA/mM
L1	NA	0.13 ± 0.01	0.14 ± 0.01
L2	NA	0.07 ± 0.01	0.09 ± 0.02
1	72.67 ± 4.10	0.31 ± 0.02	0.19 ± 0.01
2	45.30 ± 4.49	0.50 ± 0.01	0.30 ± 0.02
BHT	4.20 ± 0.02	–	–

dimensional (2D) fingerprint, which will provide us the summary of the intermolecular contacts in the crystal structure. The Hirshfeld surfaces of complexes **1** and **2** are shown in Fig. 3, in which we have illustrated various Hirshfeld surface mapping having d_{norm}, shape index, and curvedness. The inter-contacts are highlighted by conventional mapping of d_{norm} on molecular Hirshfeld surfaces as shown in Fig. 4. The red spots over the surface indicate the closeness of atoms to the Hirshfeld surface to outside, meaning a strong hydrogen bonding between the Hirshfeld surface and the nearest atoms outside (Fig. 4). White and blue color on the surface indicates the intermediate and little proximity between the atoms involved (Fig. 4). In other words, the major hydrogen bonding interactions such as O—H···Cl, N—H···N and N—H···Cl in **1**, and O—H···O and N—H···O in **2**, involving various functionalities, anion, and solvent in the complexes, can be seen in the Hirshfeld surface as the red areas (Fig. 4). Furthermore, we have analyzed the contributions of various elements (by plotting a 2D fingerprint) and its inter contacts to the Hirshfeld surfaces of **1** and **2**, which resulted in H···H (66.0%), H···Cl (10.9%), C···H (6.3%), O···H (1.3%) and N···H (1.7%) interactions, for **1**, and H···H (47.9%), C···H (7.3%), O···H (12.2%) and N···H (1.4%) interactions for **2** (Figs. 5 and 6). In **1** and **2**, there are two sharp spikes in the lower left area of the fingerprint plot, that are belonged to O—H···Cl/N—H···Cl, and O—H···O/N—H···O, respectively ($d_i + d_e$ = 2.2 and 1.90 for **1** and **2**, respectively).

3.5. Antioxidant activity

The antioxidant activity of the synthesized ligands (**L1** and **L2**) and their complexes (**1** and **2**) has been systematically evaluated using three different assays at different concentration ranges. The scavenger capacity is determined by measuring the decrease in the absorption of the DPPH and ABTS radicals, and the results were compared with that of standard antioxidants including the synthetic antioxidant BHT (Butylated Hydroxy Toluene), ascorbic acid and Trolox. Meanwhile, we have also evaluated the ability of synthesized compounds to reduce Fe^{3+} to Fe^{2+} by using the Ferric Reducing Antioxidant Power (FRAP) test. These three assays are mainly used to measure the direct involvement of the compound in improving the primary antioxidant activity.

One of the most widely used methods for evaluating total antioxidant activity is the determination of DPPH· trapping activity by its simple, rapid, sensitive and reproducible procedure. The DPPH reagent allows us to determine the intrinsic capacity of a substance having groups (RH) such as phenols to give a hydrogen atom or electrons. In our study (Table 3), Complexes **1** and **2** present a promising free DPPH scavenging capacity with IC_{50} values of 45.30 and 72.67 μM, respectively, compared to BHT (4.2 μM).

The ABTS method is based on the ability of hydrogen or electron-donating antioxidants to decolorize the performed radical monocation of 2,2′-azino-bis(3-ethyl-benzthiazoline-6-sulfonic acid) generated due to oxidation of ABTS with potassium persulfate. The radical scavenging

abilities showed by the tested compounds towards this assay typically revealed that, the two complexes **1** and **2** exhibit significantly better activity, expressed as trolox equivalents (μM Trolox/mM of compound) with 0.31 and 0.50 trolox equivalents, respectively (Table 3). Whereas, the two ligands **L1** and **L2** allow the moderate radical scavenging ability with values 0.13 and 0.07 trolox equivalents, respectively.

Subsequently, we also evaluated the capacity of the synthesized compounds for reducing Fe^{3+} to Fe^{2+} by employing the ferric reducing antioxidant power (FRAP) test [33]. The complex **2** displays the higher effect in reducing ferric to ferrous iron, expressed as ascorbic acid (AA) equivalents (μM AA/mM of compound) reaching more than 0.30 ascorbic acid equivalents (Table 3). Thus, the ligand **L1** and complex **1** had moderate effect with 0.14 and 0.19 ascorbic acid equivalents. However, the complex **2** had a minimum effect in reducing ferric iron, with value 0.09 ascorbic acid equivalents.

4. Conclusion

Two pyrazole-acetamide ligands (**L1** [35] and the new **L2**) were studied for their coordination/chelation and crystallization properties with $CoCl_2$ and $CuSO_4$, which lead to the formation of two new mononuclear complexes, $[Co(\mathbf{L1})_2(EtOH)_2]\cdot Cl_2$ (**1**) and $[Cu(\mathbf{L2})]\cdot H_2O$ (**2**). Single crystal X-ray diffraction structural analysis of these two complexes exposed the role of intermolecular hydrogen bonding interactions, to determine their supramolecular network topology. The O—H···Cl and N—H···Cl hydrogen bonding interactions benefits to **1**, which is the first coordination complex with **L1**, to assemble to form a 1D chain as the primary supramolecular architecture. C—H···π(ring) interaction involving the six membered aromatic rings allows, 1D chains to be packed in parallel fashion, which resulted in a 2D sheet structure, with the encapsulation of Cl^- within the void space. On the other hand in complex **2**, O—H···O and N—H···O hydrogen bonding play a role to self assemble the crystallographically independent molecules of complexes and water molecules to form a 2D corrugated hydrogen bonded sheet. Furthermore, the ligands and its complexes were investigated for their antioxidant activity by examining their *in vitro* ability to scavenge free radicals such as DPPH, ABTS and FRAP. The results revealed that the ligands and their complexes exhibited significant antioxidant capacity compared to literature references.

Abbreviations

AA	ascorbic acid
ABTS	2,2′-azino-bis(3-ethylbenzothiazoline-6-sulphonic acid
ATR	attenuated total reflection
BHT	Butylated Hydroxy Toluene
CCD	charge-coupled device
CCDC	Cambridge Crystallographic Data Centre
DPPH	1,1-diphenyl-2-picrylhydrazyl
DHA	dehydroacetic acid
ESI-MS	electrospray ionization-mass spectrometry
EtOH	ethanol
FRAP	Ferric Reducing Antioxidant Power
IR	infrared spectrophotometry
IC50	half maximal inhibitory concentration
NMR	nuclear magnetic resonance spectroscopy
ROS	reactive oxygen species

Acknowledgments

This work was supported by a bilateral WBI action with Morocco (COP 22 Program 2018-2022), and the Fonds De La Recherche Scientifique - FNRS (PDR T.0102.15).

References

[1] K. Karrouchi, S. Radi, Y. Ramli, J. Taoufik, Y.N. Mabkhot, F.A. Al-aizari, M. Ansar, Molecules 23 (2018) 134.
[2] K.R.A. Abdellatif, W.A.A. Fadaly, Y.A.M. Elshaier, W.A.M. Ali, G.M. Kamel, Bioorg. Chem. 77 (2018) 568–578.
[3] M.A. Abdelgawad, M.B. Labib, M. Abdel-Latif, Bioorg. Chem. 74 (2017) 212–220.
[4] A. Çetin, İ. Bildirici, J. Saudi Chem. Soc. 22 (2018) 279–296.
[5] O.I. El-Sabbagh, M.M. Baraka, S.M. Ibrahim, C. Pannecouque, G. Andrei, R. Snoeck, J. Balzarini, A.A. Rashad, Eur. J. Med. Chem. 44 (2009) 3746–3753.
[6] K. Karrouchi, L. Chemlal, J. Taoufik, Y. Cherrah, S. Radi, M. El Abbes Faouzi, M. Ansar, Ann. Pharm. Fr. 74 (2016) 431–438.
[7] E. Guillén, A. González, P.K. Basu, A. Ghosh, M. Font-Bardia, T. Calvet, C. Calvis, R. Messeguer, C. López, J. Organomet. Chem. 828 (2017) 122–132.
[8] K. Karrouchi, E.B. Yousfi, N.K. Sebbar, Y. Ramli, J. Taoufik, Y. Ouzidan, M. Ansar, Y.N. Mabkhot, H.A. Ghabbour, S. Radi, Int. J. Mol. Sci. 18 (2017) 2215.
[9] J.-J. Shi, G.-H. Ren, N.-J. Wu, J.-Q. Weng, T.-M. Xu, X.-H. Liu, C.-X. Tan, Chin. Chem. Lett. 28 (2017) 1727–1730.
[10] R. Narlawar, M. Pickhardt, S. Leuchtenberger, K. Baumann, S. Krause, T. Dyrks, S. Weggen, E. Mandelkow, B. Schmidt, Chem. Med. Chem. 3 (2008) 165–172.
[11] Friedrich, H.-B. Zhou, S. Sheng, D.R. Compton, Y. Kim, A. Joachimiak, S. Sharma, K.E. Carlson, B.S. Katzenellenbogen, K.W. Nettles, G.L. Greene, J.A. Katzenellenbogen, J. Med. Chem. 50 (2007) 399–403.
[12] N.R. Emmadi, C. Bingi, S.S. Kotapalli, R. Ummanni, J.B. Nanubolu, K. Atmaku, Bioorg. Med. Chem. Lett. 25 (2015) 2918–2922.
[13] G.R. Bebernitz, G. Argentieri, B. Battle, C. Brennan, B. Balkan, B.F. Burkey, M. Eckhardt, J. Gao, P. Kapa, R.J. Strohschein, H.F. Schuster, M. Wilson, D.D. Xu, J. Med. Chem. 44 (2001) 2601–2611.
[14] Z. Sun, J. Khan, M. Makowska-Grzyska, M. Zhang, J.H. Cho, C. Suebsuwong, P. Vo, D.R. Gollapalli, Y. Kim, A. Joachimiak, L. Hedstrom, G.D. Cuny, J. Med. Chem. 5 (2014) 10544–10550.
[15] P.P. Dholakiya, M.N. Patel, Synth. React. Inorg. Met.-Org. Chem. 34 (2004) 383–395.
[16] M. Jia, A. Seifert, M. Berger, H. Giegengack, S. Schulze, W.R. Thiel, Chem. Mater. 16 (2004) 877–882.
[17] J. Liu, H. Zhang, C. Chen, H. Deng, T. Lu, L. Ji, Dalton Trans. (2003) 114–119.
[18] M. Paul, N.N. Adarsh, P. Dastidar, Cryst. Growth Des. 14 (2014) 1331–1337.
[19] T. Shiga, E. Oshiro, N. Nakayama, K. Mitsumoto, G.N. Newton, H. Nishikawa, H. Oshio, Eur. J. Inorg. Chem. 56 (2013) 781–787.
[20] P. Konieczny, R. Pełka, P.M. Zieliński, F.L. Pratt, P. Pinkowicz, B. Sieklucka, T.J. Wasiutyński, J. Magn. Magn. Mater. 344 (2013) 105–108.
[21] W.L. Driessen, W.G.R. Wiesmeijer, M. Schipper-Zablotskaja, R.A.G. De Graaff, J. Reedijk, Inorg. Chim. Acta 162 (1989) 233–238.
[22] C. Dowling, V.J. Murphy, G. Parkin, Inorg. Chem. 35 (1996) 2415–2420.
[23] M. Valko, D. Leibfritz, J. Moncol, M.T.D. Cronin, M. Mazur, J. Telser, Int. J. Biochem. Cell Biol. 39 (2007) 44–84.
[24] P.D. Ray, B.-W. Huang, Y. Tsuji, Cell. Signal. 24 (2012) 981–990.
[25] E. Songül, Ş. Musa, Ö. Mustafa, R. Apak, B. Ülküseven, Inorg. Chim. Acta 469 (2018) 495–502.
[26] G. Nirmala, R. Aveli, V. Narendrula, S.D. Shivaraj, J. Mol. Struct. 1173 (2018) 173–182.
[27] K. Chkirate, R. Regragui, E.M. Essassi, M. Pierrot, Z. Kristallogr. NCS 216 (2001) 635–636.
[28] K. Chkirate, N.K. Sebbar, Y. Ouzidan, E.M. Essassi, J.T. Mague, IUCrData 2 (2017) x170285.
[29] G.M. Sheldrick, Acta Cryst C71 (2015) 3–8.
[30] C.F. Macrae, P.R. Edgington, P. McCabe, E. Pidcock, G.P. Shields, R. Taylor, M. Towler, J. Van De Streek, J. Appl. Crystallogr. 39 (2006) 453–457.
[31] T. Li, S. Li, Y. Dong, R. Zhu, Y. Liu, Food Chem. 145 (2014) 335–341.
[32] C.I.G. Tuberoso, M. Boban, E. Bifulco, D. Budimir, F.M. Pirisi, Food Chem. 140 (2013) 686–691.
[33] M. Oyaizu, J. Jpn, Nutr. Diet. 44 (1986) 307–315.
[34] M. El Abbassi, E.M. Essassi, J. Fifani, Tetrahedron Lett. 28 (1987) 1389–1392.
[35] E.M. Essassi, M. El Abbassi, J. Fifani, Bull. Soc. Chim. Belg. 96 (1987) 225–228.
[36] S.K. Wolff, D.J. Grimwood, J.J. McKinnon, M.J. Turner, D. Jayatilaka, M.A. Spackman, CrystalExplorer 3.1, University of Western Australia, Crawley, Australia, 2013.
[37] M.A. Spackman, D. Jayatilaka, CrystEngComm 11 (2009) 19–32.